Thin Solid Films 732 (2021) 138800

Contents lists available at ScienceDirect

Thin Solid Films

journal homepage: www.elsevier.com/locate/tsf

Investigation of optical, electronic, and magnetic properties of p-type NiO thin film on different substrates

Dogan Kaya [a], Hafize Seda Aydınoğlu [b], Ebru Şenadım Tüzemen [c,d], Ahmet Ekicibil [e]

[a] Department of Electronics and Automation, Vocational School of Adana, Cukurova University, 01160, Adana, Turkey
[b] Department of Medical Services and Techniques, Program of Opticianry, Vocational School of Healthcare, Sivas Cumhuriyet University, 58140, Sivas, Turkey
[c] Nanophotonics Research and Application Center, Sivas Cumhuriyet University, 58140, Sivas, Turkey
[d] Department of Physics, Faculty of Science, Sivas Cumhuriyet University, 58140, Sivas, Turkey
[5] Department of Physics, Faculty of Art and Sciences, Cukurova University, 01330, Adana, Turkey

ARTICLE INFO

Keywords:
Nickel Oxide
Thin film
Thermal evaporation
Optical properties
Hall-effect

ABSTRACT

In this study, high-quality p-type NiO semiconductor thin film was investigated using the thermal evaporation method after thermal oxidation of as-deposited 50 nm Ni film at 450°C for 2.5 h. NiO thin film simultaneously formed on substrates of different nature; glass, sapphire, Si(100), InP, and GaAs. The structural properties of NiO films were determined as cubic phase with a space group of $Fm\bar{3}m$ by X-ray diffraction analysis. We observed that the Ni ions were interacted with sapphire, InP, and GaAs substrates rather than glass and Si(100) substrates. During the annealing process, Ni ions diffused into the sapphire, InP, and GaAs substrates, and resulted in a formation of secondary phases of NiAl, Ni_xP/Ni_2InP, and $NiAs/Ni_2GaAs$. Scanning electron microscopy images managed to determine the average film thickness that is also affected by Ni-surface interactions. The optical transparency was determined to be at approximately 94% and 89% transmittance in the range of 300-800 nm for the NiO film on sapphire and glass samples, respectively. The direct optical band gap of NiO films on glass and sapphire substrates were calculated by Tauc's equation and found to be 3.63 eV and 3.67 eV, respectively. NiO films on glass and sapphire surfaces exhibited a p-type characteristic that was confirmed by Hall-effect measurements. The magnetic field dependence of magnetization was measured at 10 K and 300 K and the maximum saturation magnetization and the effective magnetic moment were recorded as 245×10^3 A/m and $2.58\mu_B$, respectively, for the NiO film on the glass at 10 K.

1. Introduction

Metal oxide materials have recently received considerable attention due to their high sensitivity, fast response/recovery times, low power consumption, and low production costs for the applications such as gas sensors, optical devices, thin-film transistors, etc. [1-3]. The formation, nucleation, and growth of these metal oxide thin-films are strongly affected by the substrate properties including surface orientation, defects, grain boundaries, and dislocations which play important role in limiting the charge carrier mobility [4]. There are several substrate textures; the thin film can be formed with no preferred growth orientation (such as on glass), with epitaxial growth (such as on $Al_2O_3(0001)$), with parallel growth (such as on the (100), (001) planes of Si, Ge) or with perpendicular to the substrate planes [4-6]. If there is no preferred growth orientation, the film growth occurs randomly. Therefore, the substrates play an important role in the film crystallinity properties to grow uniform and desirable metal oxide thin films. p-Typical p-type metal oxide semiconductors CuO, NiO, Co_3O_4, Mn_3O_4, and Cr_2O_3 are widely used because oxidation provides enhanced conduction activities near the surface and hole accumulation [7-14]. Among these p-type materials, NiO is one of the most promising materials for p-type transparent conducting oxides in the visible regime for optoelectronic devices [9], gas sensors [15], spin-valve heterostructures [16], metal-semiconducting electrodes [17], antiferromagnetic layers [18], light emitting devices [19], and organic light-emitting diodes [20]. Physical deposition of NiO thin films can be achieved by sputtering [21], pulsed laser deposition [22], electron-beam evaporation [23], atomic layer deposition [24], and oxidation of metallic Ni films [25, 26]. Among these, the thermal evaporation method is widely used for oxidation of a metallic Ni film because it is a simple and robust technique with high film coating speed, less damaging atomic collisions, and excellent purity due to high vacuum conditions [25].

Nickel is a type of hard, silver-white colored material, a readily available, and highly abundant on Earth. It also provides high conductivity lower only than Cu, Au, Ag and Pt metals, and therefore it is used in the applications with thin-film integrated inductors as electrodes for solar cells and electronic devices due to low electrical resistance and high oxidation resistance [27]. Nickel has a relatively low melting point

https://doi.org/10.1016/j.tsf.2021.138800
Received 15 February 2021; Received in revised form 14 June 2021; Accepted 16 June 2021
Available online 23 June 2021

of ~1453°C in the air and ~1070°C at 1.33 10^{-4} Pa vacuum pressure, which allows an easy production process [26]. To produce chemically stable NiO thin films on substrates [4, 17, 28], one easy and effective method is to anneal a Ni film above 350°C in the air at which NiO peaks start to appear in X-ray diffraction (XRD) analysis [29]. With thermal evaporation method, a uniform NiO layer with a cubic structure can be produced relatively easily and, in partial or complete oxidation of the Ni film can be controlled by the Ni film thickness, annealing temperature, and time.

Bulk NiO exhibits antiferromagnetic (AFM) ordering below the Neel temperature of T_N=523 K with a cubic structure [30]. NiO is a well-known charge-transfer metal and its energy band gap can be varied between 3.2 eV and 4.2 eV depending on the preparation method, film thickness, and substrate [8, 31]. Therefore, this wide range of the NiO films' band gap in the visible regime provides great potential for use in transparent conducting oxides, spin-valve giant magnetoresistive sensors, electrochromic display devices, gas and chemical sensor applications, Schottky diodes, and metal oxide field-effect transistors (MOSFETs) [32]. In this study, we investigated the formation of NiO films via oxidizing Ni thin film at 450°C for 2.5 h in the air by thermal evaporation method on glass, Si(100), sapphire, InP, and GaAs substrates. By these means, we aim to understand the structural and morphological properties of NiO thin films on different types of substrates via XRD, scanning electron microscopy (SEM), and energy-dispersive X-ray spectroscopy (EDS) analyses. Further, we aim to determine the optical and electronic properties of NiO film by ultraviolet-visible-near infrared (UV–VIS–NIR) spectrophotometry and Hall effect measurements to control the oxidation process. The magnetic field dependence of the magnetization curves support understanding the structural formations.

2. Experimental Method

The process of NiO film formation on the substrates was performed as follows: 50 nm Ni film was deposited by the thermal evaporation method. While the sample holder rotates with 10 rpm to produce uniform film thickness, Ni pellets in tantalum boat with a purity of 99.99% were evaporated with an evaporation power of 300 W that resulted in 0.1 Å/s growth rate at a temperature of 30 °C and a base pressure of ~1.96 10^{-4} Pa. We used different natures of substrates that were cut into small pieces of 10 mm × 10 mm size: glass, Si(100), sapphire (Al_2O_3(0001)), InP, and GaAs substrates. No intentional heating was applied to the substrate holder before or during thin film growth. Following this, the Ni (50 nm) film on the substrates was annealed at 450°C for 2.5 h in the air and the Ni layer was fully oxidized and formed a NiO layer. After NiO formation, the films were placed back into the evaporation system to deposit the Ti layer that is used as a cap on the NiO layer to protect from further oxidation and film cracks. While the sample holder rotates with 10 rpm, 15 nm of Ti layer were deposited with a purity of 99.99% Ti target by using radio frequency (RF) magnetron sputtering method with a power of 118 W that induced 0.3 Å/s at a temperature of 30°C and base pressure of ~4 Pa. The thicknesses of the Ni and Ti films were determined by a quartz crystal oscillator close to the sample holder during the deposition, and the distance between the sources and the sample holders was 25 cm and 11 cm, respectively.

The structural analyses of NiO films on substrates were performed with a PANaylitical EMPYREAN XRD system that uses Bragg-Brentano geometry with Cu-Kα radiation (λ=1.54 Å) in which the working voltage and current were set as at 45 kV and 40 mA, respectively. The morphology and thickness of the thin films were investigated by using FEI SEM images at 20 kV and EDS data was collected at 20 kV for 49 s at 40000 × magnification and resolution of 137 eV to confirm impurity-free thin film formation of samples. Optical characterization of the NiO films was carried out using a double-beam UV–VIS–NIR spectrophotometer (Cary 5000). Optical transmission spectra were taken in the wavelength range of 390–800 nm using a solid sample holder accessory. Hall effect measurement were performed by applying a magnetic field of 0.1 T, current of 100 nA, and voltage of 5 V. A variable temperature Quantum Design physical property measurement system with a vibrating sample magnetometer was used for the magnetic field dependent measurements with an applied magnetic field up to ±3 T between the temperature of 10 K and 300 K.

3. Results and Discussions

We prepared two samples on a glass substrate: 50 nm of Ni thin film as a control sample and oxidized Ni film to form NiO film on the glass substrate. The XRD results of these samples are presented in Fig. 1(a). Although the as-prepared Ni film (red line) exhibits amorphous phase formation rather than crystalline nature, the formation of the NiO film (black line) appears with major peaks after annealing the sample at 450°C for 2.5 h in the air. We obtained a very weak signal to background noise ratio but complete oxidation without Ni peaks and cubic phase with a space group of $Fm\bar{3}m$ for the NiO film [29]. Three major peaks of NiO sample were observed at 2θ=37.3°, 43.3° and 62.7° that correspond to the crystal planes of the (111), (200) and (220), respectively [15, 16]. EDS analysis of NiO sample on glass substrate was given in Fig. 1(b) with major signals of Si (●) (%45.1), O (%53.5), Ni (%1.2), and Ti (%0.2) [33]. We can conclude from the XRD patterns and EDS analysis that no other impurity peaks were detected in the sample. Further investigation with SEM are shown in Fig. 1(c) on which uniform and flat thin film formation was obtained and the average film thickness of NiO is found to be 45.7 ± 4.6 nm. Fig. 1(d) shows an area of EDS analysis and percentages of elemental atomic which were detected in the image frame.

The XRD peaks at the scattering angles (two theta) of the NiO thin film on (a) Si(100), (b) sapphire, (c) InP, and (d) GaAs substrates after simultaneous deposition and annealing are presented in Fig. 2. The crystalline formation of the NiO film on the Si(100) surface (see Fig. 2 (a)) was obtained. The cubic phase with space group $Fm\bar{3}m$ of NiO film peaks at 2θ=37.3°, 43.3° and 61.6° assigned to the (111), (200) and (220) planes are similar to the NiO film formation on a glass substrate [26]. Here, the peaks at 2θ=32.9°, 61.6° and 68.9° belong to the Si(100) substrate and these peaks correspond to the Miller indices of (100), (320) and (400), respectively [34]. The XRD patterns further confirm that the NiO film grows on the Si(100) surface with high purity. However, the Ni ions do not interact with the substrate atoms, so we did not observe the Ni-Si phase in the XRD pattern. As can be seen in Fig. 2(b), similar major peaks of the NiO film at 2θ=37.3°, 43.3°, 62.8° and 80.1° were observed that correspond to the (111), (200), (220) and (222) planes along with the major peaks belong to sapphire substrate (Al_2O_3(0001)) at 2θ=41.4° and 90.7° [35]. The sapphire substrate provides the out-of-plane surface orientation on which the NiO thin film grows on the (111) and (222) planes [28, 36]. There is an additional phase (marked with ▲) at 2θ=64.6° which may be assigned to NiAl phases [37]. The annealing process at 450°C may result in further diffusion of Ni ions into the substrate, so the formation of NiAl phase occurs along with NiO phases.

The annealing process for the Ni film on InP substrate results in more complicated phases, which is shown in Fig. 2(c). The characteristic peaks of NiO are at 2θ=36.0°, 42.2° and 80.0° with a small shift due to the InP substrate. Moreover, the peaks of InP which are at 2θ=30.3°, 63.1° and 100° represents the (002), (004) and (4-2-22) reflection planes, respectively. A recent study by Ghegin *et al.* investigated the Ni film formation on the InP surface as a function of temperature from 250°C to 550°C [17]. The results showed that the formation of Ni_xP and Ni_2InP phases in the structure is possible along with NiO formation. This study concluded that annealing above 250°C results in Ni ions diffusing into the substrate and forming Ni_2InP, Ni_3P, and Ni_2P phases (* marks in Fig. 2(c)). These peaks are identified as Ni_3P at 27.3°, Ni_2InP at 38.7°, and Ni_2P at 44.4° and 56.5°. Here we could not identify the peak at

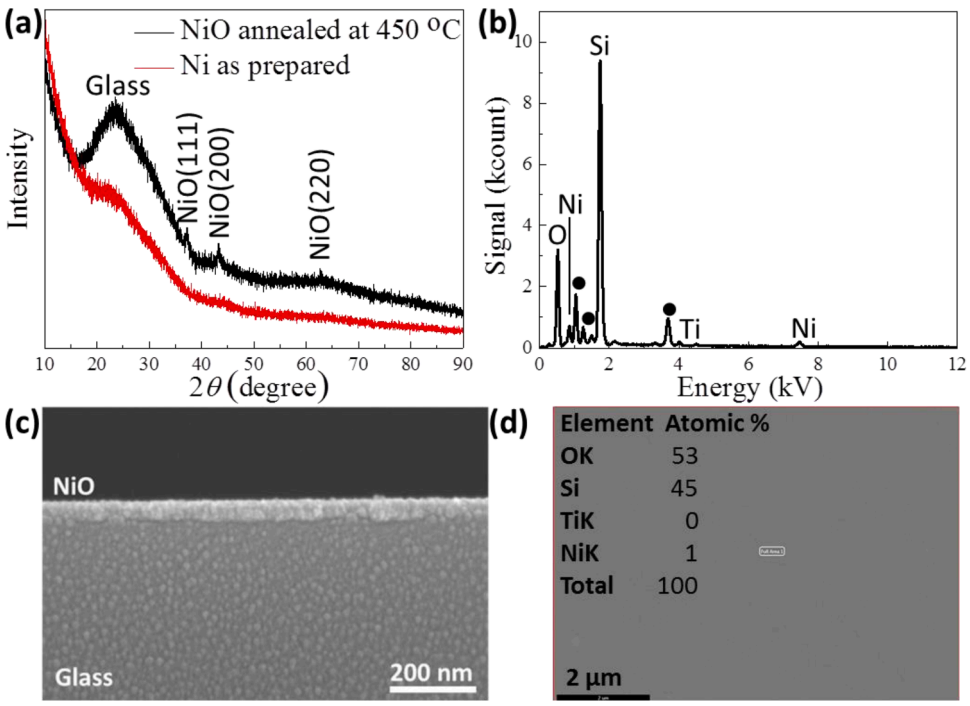

Fig. 1. (a) XRD data of Ti/Ni (red as prepared sample) and Ti/NiO (black oxidized sample at 450°C for 2.5 h) on glass substrate. (b) EDS data with possible atomic intensities. (c) SEM image of NiO film on the substrate with a thickness of 45.7 ± 4.6 nm. (d) Elemental atomic percentages of EDS data for a selected area.

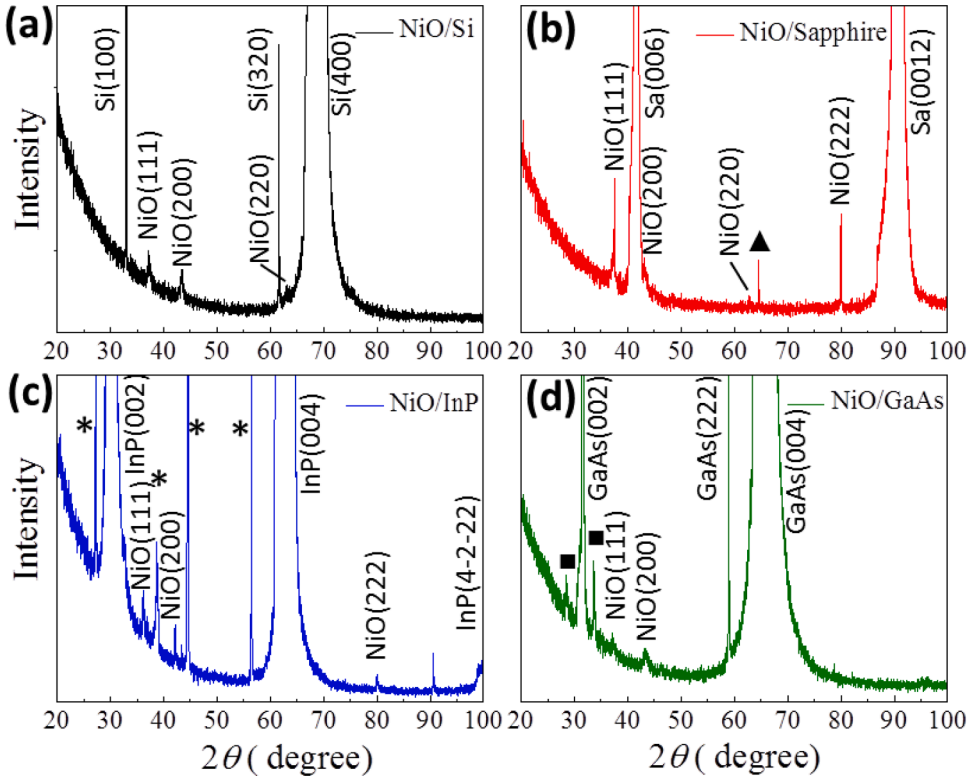

Fig. 2. The XRD patterns of oxidized Ni layer at 450°C for 2.5 h in the air on (a) Si(100) (black line), (b) Sapphire (red line), (c) InP (blue line) and (d) GaAs (green line) substrates. Along with major NiO and substrate peaks, geometric marks indicate NiAl (▲),Ni_2InP, Ni_3P, and Ni_2P (*), and NiAs and Ni_2GaAs (■) phases.

90.5°, which may also arise from the Ni ions and the substrate interaction. The NiO growth on GaAs substrate is presented in Fig. 2(d). The NiO peaks at 2θ=37.2° and 43.2° belong to the (111) and (200) planes. Here the (220) plane at around 2θ=62.7° were suppressed by the major GaAs peak of (004) plane. Along with the major NiO and GaAs peaks, there are additional peaks at 28.6° and 33.6° which correspond to NiAs and Ni_2GaAs phases (■ marks in Fig. 2(d)) [38]. A similar diffusion mechanism has been observed for Ni ions that diffuse into the GaAs substrate via thermal activation at 450°C [39]. The formation of NiO crystalline planes is highly dependent on the substrate crystal

orientation, defects, grain boundaries, dislocations, and annealing temperature of Ni film [17, 29, 40, 41]. While the (222) plane was formed for sapphire and InP substrates, the annealing temperature of 450°C is not enough to form the (222) planes for both Si(100) and GaAs substrates. A recent study has investigated the NiO formation on GaAs substrate as a function of temperature and the XRD data showed that the (222) plane of NiO film appears at 600°C [40]. Overall, we did not observe Ti peaks in all samples.

We collected SEM images to characterize the NiO film thickness on each substrate. Fig. 3 shows the formation of NiO film on (a) Si(100), (b) Sapphire, (c) InP, and (d) GaAs substrates. We measured the average film thickness of the NiO layer as 62.6 ± 5.4 nm, 71.1 ± 4.3 nm, 31.2 ± 2.2 nm, and 54.2 ± 4.5 nm for Si(100), Sapphire, InP, and GaAs substrates, respectively. The different film thicknesses obtained for NiO may arise from the Ni ions interaction with substrates and oxygen during the thermal annealing process. Specifically, Ni ions diffuse in InP and GaAs substrates and form Ni_xP/Ni_2InP, and $NiAs/Ni_2GaAs$ phases, respectively.

Further, Fig. 4 presents EDS analysis of oxidized Ni films on (a) Si (100), (b) Sapphire, (c) InP, and (d) GaAs substrates. Inset images show the selected EDS data of SEM images and elemental analysis results of the compositions that were collected on the selected point. Similar atomic percentages of Ni, O, Ti, and substrate contributions were observed at three different points of the film and the average value of Ni contents was between 0.4% and 2.9%, Ti contents were between 0.14% and 0.39% and the substrate contributions were about 90%. The SEM images collected during EDS analysis revealed that, after oxidizing the Ni film on the top of the NiO surface is reasonably smooth.

The proposed growth mechanism of NiO thin films on glass, Si(100), sapphire, InP, and GaAs substrates is presented in Fig. 5. The sample preparation started with the deposition of a 50 nm Ni layer on the substrates (left). Here, we did not increase the substrate temperature to prevent any Ni-substrate interaction during deposition. However, oxidation processes at 450°C for 2.5 h in the air result in the Ni film interaction with and without the substrates (center). Choosing an annealing temperature of 450°C led to complete oxidation of the Ni layer in 2.5 h by diffusion of oxygen ions from air and then the substrates through created cracks and microchannels into the Ni layer. At this stage, we observed two different pathways: Ni ions interactions with glass and Si(100) and without sapphire, InP, and GaAs substrate interactions. The possible ion exchanges between Ni and substrate atoms for sapphire, InP, and GaAs were confirmed though XRD analysis and the SEM images. The thermal oxidation reaction, that is $Ni+1/2O_2 \rightarrow NiO$, may increase the film thickness of NiO/Si(100) and Sapphire as found to be 62.6 ± 5.4 nm and 71.1 ± 4.3 nm, respectively. The XRD analysis also indicates that Ni ions can diffuse into InP or GaAs substrates and form other phases such as NiAl, Ni_2InP, Ni_3P, Ni_2P, NiAs, and Ni_2GaAs. Overall, the annealing process resulted in NiO formation on glass and Si(100) substrates without interacting with Ni ions as confirmed by the XRD analysis. Sapphire, InP, and GaAs substrates interacted with Ni during the annealing process and formed NiAl, Ni_xP/Ni_2InP, and $NiAs/Ni_2GaAs$ phases, respectively. In the end, we deposited 15 nm of Ti layer on the top of the NiO film (right). While the p-type NiO formation on glass and sapphire substrates provides possible optoelectronic applications due to the transparent substrate properties, the interaction between Ni and InP and GaAs can be a good candidate for microelectronic applications such as contact for Schottky diodes or MOSFETs with improved thermal and electrical stability, as well as desirable morphologies.

The optical transparency and the optical band gap analyses of NiO thin films on glass and sapphire samples were performed using a Cary 5000 UV-VIS-NIR spectrophotometer system with a wavelength range between 175 nm-3300 nm. The transmittance of the films on glass (black line) and sapphire (red line) is plotted in Fig. 6(a) as a function of wavelength. It can be seen from the figure that the transmittance of the sample grown on sapphire is higher than that of glass. We observed approximately 94% and 89% transmittance in the range of 300-800 nm for NiO on sapphire and glass samples, respectively. These results indicate that the film on sapphire is more transparent and provides a promising percentage for optical applications. Since NiO film on sapphire has an ordered crystalline structure, which is confirmed by XRD results, the high transmittance also arises from this ordered crystal formation on sapphire compared to glass substrates in this study.

The optical band gap of semiconductor materials is important for optoelectronic applications and it can be determined from the electron excitation from the valance band to the conduction band of the film [36]. Optical transitions in ideal semiconductor materials occur as direct and indirect transitions. The absorption coefficient is given by the

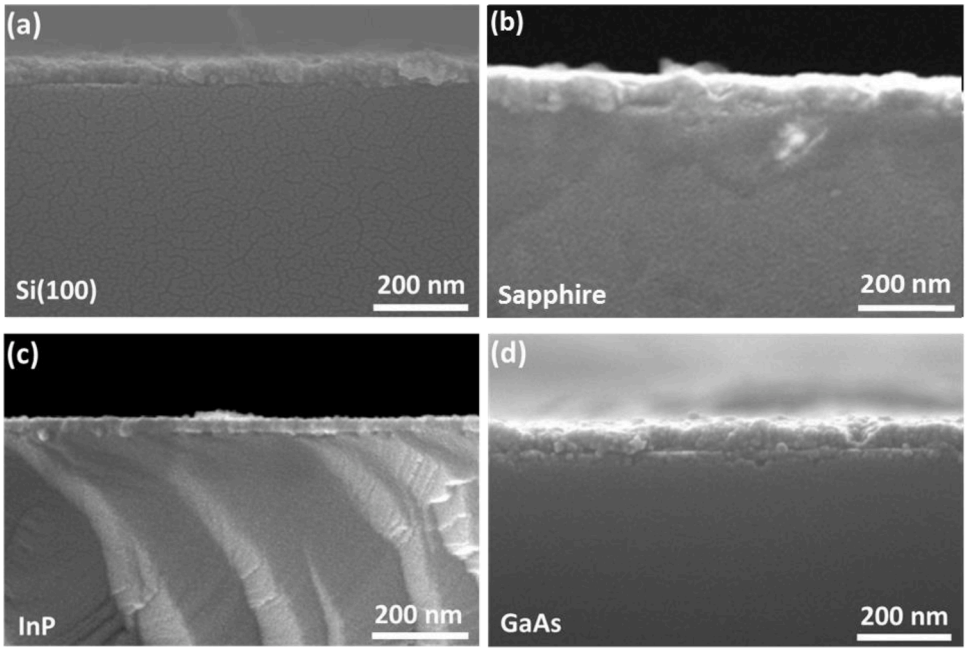

Fig. 3. SEM images of oxidized Ni layer at 450°C for 2.5 h in the air on (a) Si(100), (b) Sapphire, (c) InP, and (d) GaAs substrates.

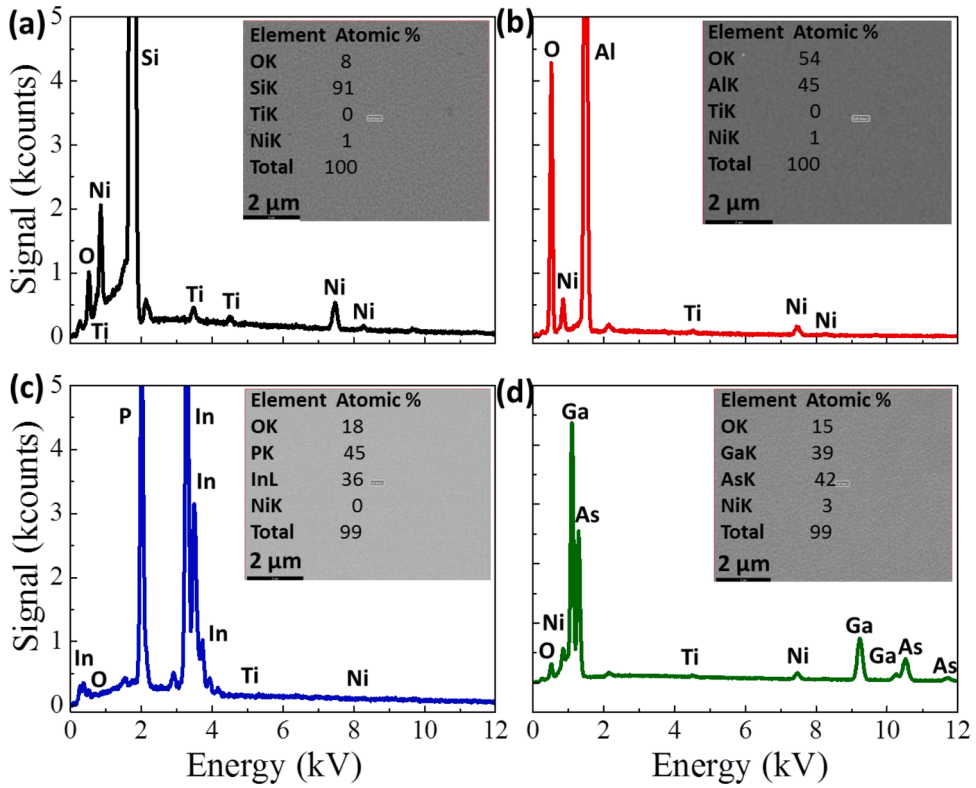

Fig. 4. EDS analysis of oxidized Ni layer on (a) Si(100), (b) Sapphire, (c) InP and (d) GaAs substrates. Inset images show selected data points with elemental analysis results of the compositions.

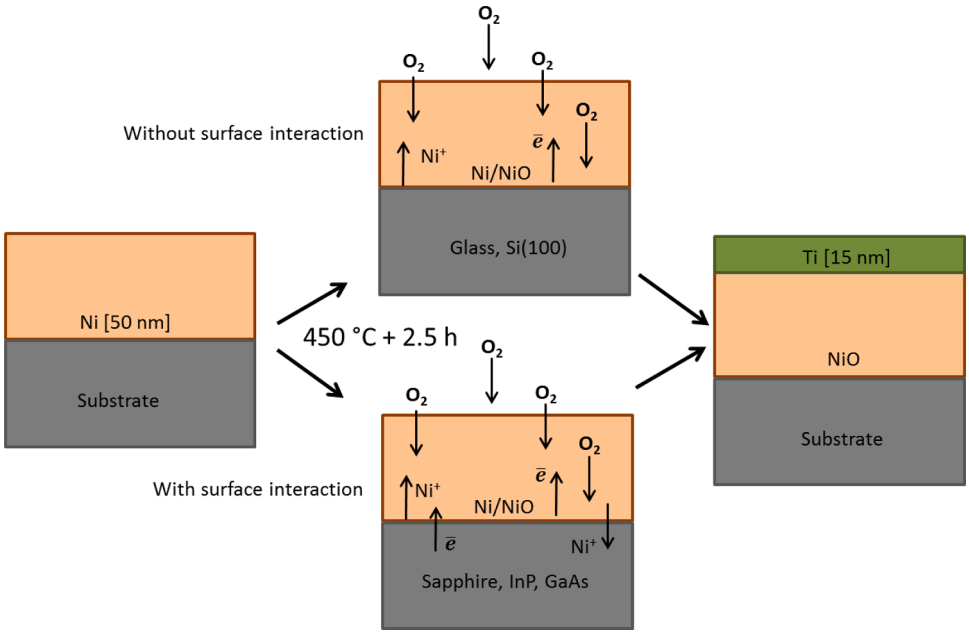

Fig. 5. Sample preparation processes: (left) Ni (50 nm) deposition on substrates, (center) annealing at 450°C for 2.5 h in the air, and (right) deposition Ti (15 nm) on NiO layer.

well-known Tauc's equation [42]

$$\alpha h\nu = B\left(h\nu - E_g\right)^m$$

$$\alpha E = B\left(E - E_g\right)^m$$

where α is the absorption coefficient, B is an independent energy constant, E_g is the energy band gap, and m is a constant determining the type of optical transition. Here, m=2 for indirect permitted passage, m=3 for indirect prohibited passage, m=1/2 for direct permitted passage, and m=3/2 for direct prohibited passage. Since NiO has a direct energy band gap, therefore, it is taken as m=1/2.

Plotting $(\alpha E)^2$ as a function of $h\nu$ is vital to find the energy band gap, E_g, of NiO thin films grown on glass and sapphire (see Fig. 6(b)). Then,

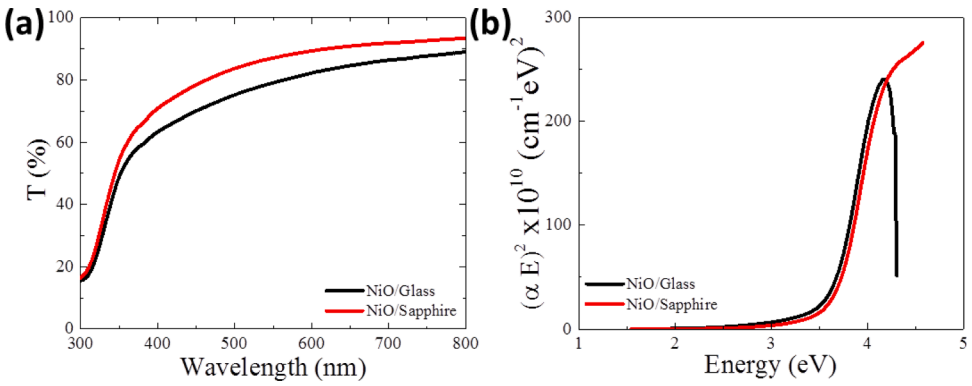

Fig. 6. Optical analysis of oxidized Ni layer at 450 C for 2.5 h on glass (black line) and sapphire (red line) (a) transmittance vs. wavelength in a range of 300-800 nm (b) $(\alpha E)^2$ vs. energy plots.

the energy band gap was found by taking the place where the graph cuts the energy axis. We calculated the band gap as 3.63 ±0.02 eV and 3.67 ±0.02 eV for glass and sapphire substrates, respectively. Under the same deposition conditions, the NiO thin film growing on sapphire always show a larger band gap than on glass. This can be due to the high-quality crystal growth of NiO film on sapphire, which is confirmed by the XRD analysis. The energy band gaps at around 3.6 eV are similar to the earlier findings, which are reported in Table 1. The band gaps vary from 3.24 eV to 4.2 eV as a function of preparation methods and type of substrates as well as thickness. For example, thermally annealing 200 nm Ni film at 500°C to form NiO film on ITO (tin-doped indium oxide) coated glass substrate by thermal evaporation revealed that the optical band gap varied in a range of 3.54-6.69 eV as a function of annealing time [43] which is rather similar to our findings. Also, the average particle size, 126 nm, of NiO particles, prepared with the sol-gel technique, exhibited an optical band gap of 3.3-3.4 eV. This reduction of energy may arise from the reduced size and monodisperse particles in the structures. Due to the non-transparent substrate properties of InP and GaAs and very thin NiO film thickness (below 70 nm), we expected that the transmittance was highly reduced with comparing to NiO film on glass and sapphire substrates [44, 45]. A recent study showed that a maximum of 30% transmittance was observed for the p-NiO film on GaAs substrates [44]. Further, the optical band gap for NiO films on GaAs was calculated to be in the range of 3.54 eV for as-prepared NiO and 3.48 eV for annealed at 250°C. UV–Vis reflectance spectra of NiO film (390 nm thickness) prepared on GaAs confirmed that the signal vanished at 335 nm wavelength at which corresponds to the band gap of NiO film around 3.7 e [46]. Experimental results for the formation of NiO (320 nm thickness) on GaAs substrate confirmed that the ideality factor and barrier height were determined to be 2.21 and 0.76 eV at 300 K, respectively [47]. Similar findings were observed for NiO film on InP substrate. While the reflection for a polished InP substrate and 70 nm of NiO film on InP substrate was reduced from 32.7% to 10.0%, respectively, the transmittance is found to be 40% at wavelengths <650 nm wavelength [45].

Table 1
The comparison of the production methods, deposited surfaces, and energy band gap (eV) of NiO.

Method	Substrate	Energy band gap (eV)	Reference
Thermal evaporation	Glass	~3.63	In this study
Thermal evaporation	Sapphire	~3.67	In this study
Sol-gel technique	-	~3.3–3.4	[48]
Spin-coating technique	Glass	~3.55–3.94	[49]
Thermal evaporation	ITO coated glass	~3.69	[43]
Sol-gel spin coating	Si(100)	~3.31	[50]
Electrochemical deposition	Conducting substrate	~3.31	[51]
RF magnetron sputtering	Sapphire and corning 1737 glass	~3.24–3.79	[52]
Spray Pyrolysis	Glass	~3.38–3.94	[53]
Sol-gel spin coating	Si(100)	~3.31–3.85	[8]
Vacuum evaporator	Glass	~3.5	[54]
Vacuum evaporator	Sapphire	~4.2	[54]

Hall effect measurements were performed at room temperature to investigate the electrical properties of the films. Van der Pauw geometry was used to measure the Hall voltage and resistance. Gold contacts were used with masks prepared according to Van der Pauw geometry. The formation of the ohmic contacts was confirmed before the Hall measurements and ohmic contacts were taken. During the measurements, a magnetic field of 0.1 T, 100 nA current, and 5 V voltage were applied and results were summarized in Table 2. The conduction mechanism of NiO film strongly depends on the oxidation process of Ni and the substrate. We observed high sheet carrier density, bulk carrier, and resistivity of the NiO film on sapphire. Hall effect measurements indicate that NiO films on glass and sapphire surfaces exhibit typical p-type semiconductor behavior [30]. While the O_2 molecules diffuse through the Ni film during the annealing process, statistically the number of the Ni^{2+} ions oxidizes and form Ni^{3+} via sharing electrons between O and Ni. In this oxidation process, the vacancy of Ni leads to the formation of holes of oxygen orbitals close to Ni sites near the surface that create the p-type semiconductor of NiO film [55]. This behavior is attributed to either Ni^{2+} cationic vacancies or oxygen interstitials [56]. The resistivity of NiO was found to be around ~3.15 Ωcm and ~4.71 Ωcm, which are lower than RF magnetron sputtering assisted growth of NiO film on glass and Si(100) of ~8.5 Ωcm [56].

Fig. 7 shows the magnetic field dependence of magnetization curves (M-H) that were measured for the NiO films on glass (a) and sapphire (b) surfaces at 10 K and 300 K without a cooling field. We normalized the magnetic moment as a function of film volumes and the maximum saturation magnetizations of NiO on glass and sapphire at 10 K were found to be 245 × 10^3 A/m and 94 × 10^3 A/m, respectively. While NiO film on glass was saturated beyond 1 T applied field as seen in Fig. 7(a), we observed a reduced magnetization for NiO film on the sapphire

Table 2
Summary of Hall effect measurements of NiO on glass and sapphire given sheet carrier density, bulk carrier, mobility, resistivity, and carrier type.

Sample Name	Sheet Carrier Density ($1/cm^2$)	Bulk Carrier ($1/cm^3$)	Mobility (cm^2/Vs)	Resistivity (Ωcm)	Carrier type
GlassNi450	1.10 × 10^{10}	2.1918 × 10^{15}	883.839	3.15218	p
SapphireNi450	5.85 × 10^{10}	1.17043 × 10^{16}	116.497	4.71559	p

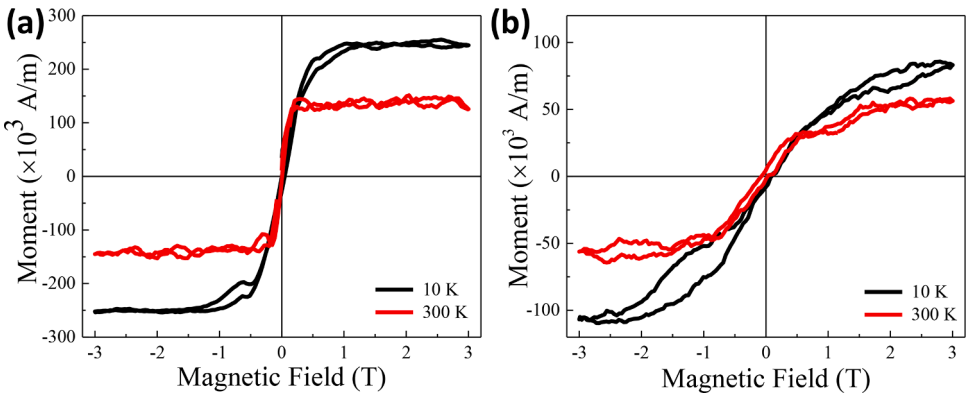

Fig. 7. Magnetic moment as a function of applied field up to 3 T for NiO on glass (a) and sapphire (b) surfaces at 10 K and 300 K.

surface and could not reach full saturation up to 3 T (Fig. 7(b)). We also observed a negative vertical hysteresis loop shift for NiO on sapphire at 10 K. This shift is called pinned magnetization, which usually occurs between FM/nonmagnetic/AFM interfaces due to AFM coupling at small or no cooling fields [57]. Both the reduction and the shift may be because of nonmagnetic NiAl formation in the structure [58], which is also confirmed by the XRD analysis in this study. We further calculated the effective magnetic moment via $\mu_{eff}=(MM_S)/(N_A\beta)$ formula. Here, M is the molecular weight of the samples, M_S is saturation magnetization of the sample, N_A is Avogadro's number, and β is a conversion factor of 9.27×10^{-24} J/T. The maximum μ_{eff} is found to be $2.58\mu_B$ for NiO on glass at 10 K and is quite similar to earlier findings of $2.87\mu_B$ per NiO unit [30]. μ_{eff} was decreased to $0.58\mu_B$ for sapphire surface due to the formation of nonmagnetic NiAl in the structure.

4. Conclusion

Fabrication of NiO thin films has been achieved by thermal evaporation of 50 nm Ni layer and annealing process at 450°C for 2.5 h in the air resulted in complete oxidized Ni film on glass, Si(100), sapphire, InP, and GaAs. The XRD results revealed the cubic phase with space group $Fm\bar{3}m$ of NiO film on all surfaces without any impurities in the film formation. Although sapphire, InP, and GaAs surfaces interacted via Ni ions diffusing into the substrate during the annealing process, Ni interaction was not observed for the glass and Si(100) surfaces. This diffusion resulted in NiAl, Ni_xP/Ni_2InP, and $NiAs/Ni_2GaAs$ phases, which also affected the average film thickness. Using UV-VIS-NIR spectrophotometer, the optical transparency of the NiO films on the glass and sapphire surfaces was determined as a function of wavelength between 300-800 nm and we observed enhanced transmittance for NiO on sapphire as 94%. Following this, the direct optical band gaps were calculated as 3.63 ±0.02 eV and 3.67 ±0.02 eV for NiO on glass and sapphire substrates, respectively. Hall effect measurements confirmed that both glass and sapphire samples exhibit p-type semiconductor behavior. Optical, XRD, and magnetic measurements confirmed the formation of Ni ions and substrate interactions for the sapphire substrate.

CRediT authorship contribution statement

Dogan Kaya: Conceptualization, Data curation, Methodology, Supervision, Writing - original draft, Writing - review & editing. **Hafize Seda Aydınoğlu:** Data curation, Methodology, Writing - original draft. **Ebru Şenadım Tüzemen:** Conceptualization, Data curation, Methodology, Supervision, Writing - original draft, Writing - review & editing. **Ahmet Ekicibil:** Conceptualization, Data curation, Methodology, Supervision, Writing - original draft, Writing - review & editing.

Declaration of Competing Interest

The authors declare that they have no known competing financial interests or personal relationships that could have appeared to influence the work reported in this paper.

Acknowledgements

This study was conducted in Sivas Cumhuriyet University R&D Center (CUTAM), Sivas Cumhuriyet University Nanophotonic Research and Application Center, Cukurova University Central Research Laboratory (ÇÜMERLAB).

References

[1] A. Dey, Semiconductor metal oxide gas sensors: A review, Materials Science and Engineering: B 229 (2018) 206–217.
[2] M. Gardon, J.M. Guilemany, A review on fabrication, sensing mechanisms and performance of metal oxide gas sensors, J. Mater. Sci.: Mater. Electron. 24 (2013) 1410–1421.
[3] C. Glynn, C. O'Dwyer, Solution Processable Metal Oxide Thin Film Deposition and Material Growth for Electronic and Photonic Devices, Advanced Materials Interfaces 4 (2017), 1600610.
[4] J.H. Lee, Y.H. Kwon, B.H. Kong, J.Y. Lee, H.K. Cho, Biepitaxial Growth of High-Quality Semiconducting NiO Thin Films on (0001) Al2O3 Substrates: Microstructural Characterization and Electrical Properties, Cryst. Growth Des. 12 (2012) 2495–2500.
[5] S. Suwas, R.K. Ray, Crystallographic texture of materials, Springer-Verlag London, 2014.
[6] C. Detavernier, A.S. Özcan, J. Jordan-Sweet, E.A. Stach, J. Tersoff, F.M. Ross, C. Lavoie, An off-normal fibre-like texture in thin films on single-crystal substrates, Nature 426 (2003) 641–645.
[7] H.-J. Kim, J.-H. Lee, Highly sensitive and selective gas sensors using p-type oxide semiconductors: Overview, Sensors and Actuators B: Chemical 192 (2014) 607–627.
[8] A.A. Ahmed, M.R. Hashim, M. Rashid, Control of the structural, electrical and optical properties of spin coated NiO films by varying precursor molarity, Thin Solid Films 690 (2019), 137554.
[9] M. Shkir, V. Ganesh, S. AlFaify, I.S. Yahia, H.Y. Zahran, Tailoring the linear and nonlinear optical properties of NiO thin films through Cr3+ doping, J. Mater. Sci.: Mater. Electron. 29 (2018) 6446–6457.
[10] D.P.M.D. Shaik, P. Rosaiah, O.M. Hussain, Fabrication of the Mn3O4 thin film electrodes by electron beam evaporation for supercapacitor applications, J. Electroanal. Chem. 851 (2019), 113409.
[11] P.T. Moseley, Progress in the development of semiconducting metal oxide gas sensors: a review, Meas. Sci. Technol. 28 (2017), 082001.
[12] A.A. Al-Ghamdi, W.E. Mahmoud, S.J. Yaghmour, F.M. Al-Marzouki, Structure and optical properties of nanocrystalline NiO thin film synthesized by sol–gel spin-coating method, J. Alloys Compd. 486 (2009) 9–13.
[13] K. Anandan, V. Rajendran, Morphological and size effects of NiO nanoparticles via solvothermal process and their optical properties, Mater. Sci. Semicond. Process. 14 (2011) 43–47.
[14] J. Zhao, H. Liu, Q. Zhang, Preparation of NiO nanoflakes under different calcination temperatures and their supercapacitive and optical properties, Appl. Surf. Sci. 392 (2017) 1097–1106.
[15] J. Wang, X. Wei, P. Wangyang, Gas-Sensing Devices Based on Zn-Doped NiO Two-Dimensional Grainy Films with Fast Response and Recovery for Ammonia Molecule Detection, Nanoscale Research Letters 10 (2015) 461.

[16] P. Ravikumar, B. Kisan, A. Perumal, Thickness dependent ferromagnetism in thermally decomposed NiO thin films, J. Magn. Magn. Mater. 418 (2016) 86–91.
[17] E. Ghegin, F. Nemouchi, J. Lábár, C. Perrin, K. Hoummada, S. Favier, S. Gurbán, I. Sagnes, Phase formation in the Ni/n–InP contacts for heterogeneous III/V-silicon photonic integration, Microelectron. Eng. 156 (2016) 86–90.
[18] V. Verma, M. Katiyar, Origin of intrinsic ferromagnetism in undoped antiferromagnetic NiO thin films, J. Phys. D: Appl. Phys. 48 (2015), 235003.
[19] Y. Zhang, X. Li, L. Wang, X. Yi, D. Wu, H. Zhu, G. Wang, Enhanced light emission of GaN-based diodes with a NiOx/graphene hybrid electrode, Nanoscale 4 (2012) 5852–5855.
[20] S.-W. Park, J.-M. Choi, E. Kim, S. Im, Inverted top-emitting organic light-emitting diodes using transparent conductive NiO electrode, Appl. Surf. Sci. 244 (2005) 439–443.
[21] H.-L. Chen, Y.-M. Lu, W.-S. Hwang, Characterization of sputtered NiO thin films, Surf. Coat. Technol. 198 (2005) 138–142.
[22] I. Fasaki, A. Koutoulaki, M. Kompitsas, C. Charitidis, Structural, electrical and mechanical properties of NiO thin films grown by pulsed laser deposition, Appl. Surf. Sci. 257 (2010) 429–433.
[23] D.Y. Jiang, J.M. Qin, X. Wang, S. Gao, Q.C. Liang, J.X. Zhao, Optical properties of NiO thin films fabricated by electron beam evaporation, Vacuum 86 (2012) 1083–1086.
[24] P.Antony Premkumar, M. Toeller, C. Adelmann, J. Meersschaut, A. Franquet, O. Richard, H. Tielens, B. Brijs, A. Moussa, T. Conard, H. Bender, M. Schaekers, J. A. Kittl, M. Jurczak, S. Van Elshocht, NiO Thin Films Synthesized by Atomic Layer Deposition using Ni(dmamb)2 and Ozone as Precursors, Chem. Vap. Deposition 18 (2012) 61–69.
[25] A. Echresh, M. Ali Abbasi, M. Zargar Shoushtari, M. Farbod, O. Nur, M. Willander, Optimization and characterization of NiO thin film and the influence of thickness on the electrical properties of n-ZnO nanorods/p-NiO heterojunction, Semicond. Sci. Technol. 29 (2014), 115009.
[26] D. Kaya, M. Akyol, Y. Wang, Q. Guo, F. Karadag, A. Ekicibil, Investigation of Magnetic Anisotropy in the Ni-Ge and Ni(NiO)-Ge Thin Films, J. Mol. Struct. (2020), 129662.
[27] Q. Jiang, X. Sheng, B. Shi, X. Feng, T. Xu, Nickel-Cathoded Perovskite Solar Cells, The Journal of Physical Chemistry C 118 (2014) 25878–25883.
[28] Y. Wang, J. Ghanbaja, P. Boulet, D. Horwat, J.F. Pierson, Growth, interfacial microstructure and optical properties of NiO thin films with various types of texture, Acta Mater 164 (2019) 648–653.
[29] L.D.L.S. Valladares, A. Ionescu, S. Holmes, C.H.W. Barnes, A.B. Domínguez, O. A. Quispe, J.C. González, S. Milana, M. Barbone, A.C. Ferrari, H. Ramos, Y. Majima, Characterization of Ni thin films following thermal oxidation in air, J. of Voc Sci Technol. B 32 (2014), 051808.
[30] M. Tadic, D. Nikolic, M. Panjan, G.R. Blake, Magnetic properties of NiO (nickel oxide) nanoparticles: Blocking temperature and Neel temperature, J. Alloys Compd. 647 (2015) 1061–1068.
[31] Y. Akaltun, T. Çayır, Fabrication and characterization of NiO thin films prepared by SILAR method, J. Alloys Compd. 625 (2015) 144–148.
[32] A.M. Reddy, A.S. Reddy, K.-S. Lee, P.S. Reddy, Effect of oxygen partial pressure on the structural, optical and electrical properties of sputtered NiO films, Ceram. Int. 37 (2011) 2837–2843.
[33] J. Wang, P. Yang, X. Wei, Z. Zhou, Preparation of NiO two-dimensional grainy films and their high-performance gas sensors for ammonia detection, Nanoscale research letters 10 (2015), 119-119.
[34] I.A. Tarasov, M.A. Visotin, A.S. Aleksandrovsky, N.N. Kosyrev, I.A. Yakovlev, M. S. Molokeev, A.V. Lukyanenko, A.S. Krylov, A.S. Fedorov, S.N. Varnakov, S. G. Ovchinnikov, Si/Fe flux ratio influence on growth and physical properties of polycrystalline β-FeSi2 thin films on Si(100) surface, J. Magn. Magn. Mater. 440 (2017) 144–152.
[35] J.L. Du, Y. Fang, E.G. Fu, X. Ding, K.Y. Yu, Y.G. Wang, Y.Q. Wang, J.K. Baldwin, P. P. Wang, Q. Bai, What determines the interfacial configuration of Nb/Al2O3 and Nb/MgO interface, Scientific Reports 6 (2016) 33931.
[36] P. Zhai, Q. Yi, J. Jian, H. Wang, P. Song, C. Dong, X. Lu, Y. Sun, J. Zhao, X. Dai, Y. Lou, H. Yang, G. Zou, Transparent p-type epitaxial thin films of nickel oxide, Chem. Commun. 50 (2014) 1854–1856.
[37] T. Zaharinie, R. Moshwan, F. Yusof, M. Hamdi, T. Ariga, Vacuum brazing of sapphire with Inconel 600 using Cu/Ni porous composite interlayer for gas pressure sensor application, Materials & Design 54 (1980-2015) (2014) 375–381.
[38] A. Lahav, M. Eizenberg, Y. Komem, Interfacial reactions between Ni films and GaAs, J. Appl. Phys. 60 (1986) 991–1001.
[39] S. Rabhi, C. Perrin-Pellegrino, S. Zhiou, M.C. Benoudia, M. Texier, K. Hoummada, Phase formation between Ni thin films and GaAs substrate, Scr. Mater. 141 (2017) 28–31.
[40] S.D. Singh, A. Das, M.K. Swami, U.K. Goutam, R.K. Sharma, H.S. Patel, S.K. Rai, T. Ganguli, Evaluation of interfacial structure of [111]and [001]oriented epitaxial NiO layers on GaAs substrate by non-destructive techniques, Vacuum 159 (2019) 335–340.
[41] K. Uchida, K.-i. Yoshida, D. Zhang, A. Koizumi, S. Nozaki, High-quality single crystalline NiO with twin phases grown on sapphire substrate by metalorganic vapor phase epitaxy, 2 (2012) 042154.
[42] J. Tauc, A. Menth, States in the gap, J. Non-Cryst. Solids 8 (1972) 569–585.
[43] P. Mohanty, C. Rath, P. Mallick, R. Biswal, N.C. Mishra, UV–visible studies of nickel oxide thin film grown by thermal oxidation of nickel, Physica B: Condensed Matter 405 (2010) 2711–2714.
[44] A. Özkartal, D.T. Noori, Effects of thermal annealing on the characterization of p-NiO/n-GaAs heterojunctions produced by thermal evaporation, J. Mater. Sci.: Mater. Electron. 32 (2021) 13462–13471.
[45] K. Sun, Y. Kuang, E. Verlage, B.S. Brunschwig, C.W. Tu, N.S. Lewis, Sputtered NiOx Films for Stabilization of p+n-InP Photoanodes for Solar-Driven Water Oxidation, 5 (2015) 1402276.
[46] A.A. AHMED, M. DEVARAJAN, N. AFZAL, GROWTH OF RF SPUTTERED NiO FILMS ON DIFFERENT SUBSTRATES, A COMPARATIVE STUDY 24 (2017), 1750096.
[47] G. Turgut, S. Duman, Sol–gel growth, characterization of a new p-NiO/n-GaAs structure, J. Alloys Compd. 664 (2016) 547–552.
[48] P. Mohanty, C.J. Sheppard, B.P. Doyle, E. Carleschi, A.R.E. Prinsloo, Evolution of NiO phase at the expense of metallic nickel: Structure, magnetic and electronic properties, Physica B: Condensed Matter 570 (2019) 285–290.
[49] S.T. Akinkuade, W.E. Meyer, J.M. Nel, Effects of thermal treatment on structural, optical and electrical properties of NiO thin films, Physica B: Condensed Matter 575 (2019), 411694.
[50] A.A. Ahmed, M.R. Hashim, R. Abdalrheem, M. Rashid, High-performance multicolor metal-semiconductor-metal Si photodetector enhanced by nanostructured NiO thin film, J. Alloys Compd. 798 (2019) 300–310.
[51] K. Nakaoka, J. Ueyama, K. Ogura, Semiconductor and electrochromic properties of electrochemically deposited nickel oxide films, J. Electroanal. Chem. 571 (2004) 93–99.
[52] Y. Zhao, H. Wang, F. Yang, Z. Zhen, X. Li, Q. Li, J. Li, Influence of growth temperature on structure, optical and electrical properties of nickel oxide films by magnetron sputtering, Vacuum 151 (2018) 163–166.
[53] K.O. Ukoba, A.C. Eloka-Eboka, F.L. Inambao, Experimental optimization of nanostructured nickel oxide deposited by spray pyrolysis for solar cells application, Mater. Sci. Eng., A 13 (2018) 3165–3173.
[54] K. Nama Manjunatha, S. Paul, Investigation of optical properties of nickel oxide thin films deposited on different substrates, Appl. Surf. Sci. 352 (2015) 10–15.
[55] P. Gupta, T. Dutta, S. Mal, J. Narayan, Controlled p-type to n-type conductivity transformation in NiO thin films by ultraviolet-laser irradiation, 111 (2012) 013706.
[56] S. Dewan, M. Tomar, R.P. Tandon, V. Gupta, Zn doping induced conductivity transformation in NiO films for realization of p-n homo junction diode, J. Appl. Phys. 121 (2017), 215307.
[57] M.R. Fitzsimmons, B.J. Kirby, S. Roy, Z.-P. Li, I.V. Roshchin, S.K. Sinha, I. K. Schuller, Pinned magnetization in the antiferromagnet and ferromagnet of an exchange bias system, Phys. Rev. B 75 (2007), 214412.
[58] S. Lamichhane, G.C. Kaphle, N.P. Adhikari, Electronic Structures and Magnetic Properties of NiAl and Ni3Al, 5, Quantum Matter, 2016, pp. 356–361.